The chaotic dynamics and multistability of two coupled Fitzhugh–Nagumo model neurons

Yoonsik Shim and Phil Husbands

Abstract

In this short article, we present a detailed analysis of the dynamics of a system of two coupled Fitzhugh–Nagumo neuron equations with tonic descending command signals, suitable for modelling circuits underlying the generation of motor behaviours. We conduct a search of possible attractors and calculate dynamical quantities, such as the largest Lyapunov exponents (LLEs), at a fine resolution over the areas of parameter space where complex and chaotic dynamics are most likely, to build a more detailed picture of the dynamical regimes of the system, focusing on the most complex solutions. By building a precise LLE map, we identify a narrow region of parameter space of particular interest, rich with chaotic and multistable dynamics, and show that it is on the border of criticality. This allows us to draw conclusions about possible neural mechanisms underlying the generation of chaotic dynamics. We illustrate the detailed ecology of multiple attractors in the system by listing, characterising and grouping all the stable attractors in the parameter range of interest. This allows us to pinpoint the regions with complex multistability. The greater understanding thus provided is intended to help future studies on the roles of chaotic dynamics in biological motor control, and their application in robotics, particularly by giving a deeper insight into how input signals and control parameters shape the system's dynamics which can be exploited in chaos-driven adaptation.

1. Introduction

The existence of intrinsic chaotic dynamics in the nervous system has been recognised for some time (Freeman & Viana Di Prisco, 1986; Guevara, Glass, Mackey, & Shrier, 1983; Korn & Faure, 2003; Rapp, Zimmerman, Albano, Deguzman, & Greenbaun, 1985; Terman & Rubin, 2007; Wright & Liley, 1996). Such dynamics have been shown to be integral to the operation of some neural circuits (Aihara & Matsumoto, 1982; Hoerzer, Legenstein, & Maass, 2014; Sussillo & Abbott, 2009) and in the learning and control of the dynamical interactions between brain, body and environment that are inherent in embodied behaviour (Ohgi, Morita, Loo, & Mizuike, 2008). Chaotic dynamics occur in both normal and pathological brain states, at both global and microscopic scales (Wright & Liley, 1996), and in a variety of animals, supporting the

idea that chaos plays a fundamental role in neural mechanisms. While intriguing proposals for the functional roles of neural chaos have been put forward – including for generating a kind of continual adaptive open-endedness (Skarda & Freeman, 1987), or as a means of allowing spontaneous exploration of body coordination during development (Kuniyoshi & Sangawa, 2006) – they are as yet not well understood.

The Fitzhugh–Nagumo neural model (FHN) (Fitzhugh, 1961; Nagumo, Arimoto, & Yoshizawa, 1962) has become an important tool in theoretical

Centre for Computational Neuroscience and Robotics, University of Sussex, Brighton, UK

Corresponding author:
Yoonsik Shim, Chichester I CI110, University of Sussex, Falmer, Brighton BN1 9QJ, UK.
Email: y.s.shim@sussex.ac.uk

studies of chaotic neural systems. It is a widely used two-dimensional simplification of the biophysically realistic Hodgkin–Huxley (HH) model of neural spike initiation and propagation (Hodgkin & Huxley, 1952). The HH model addresses excitation and propagation at the level of underlying cellular electrochemical processes, while FHN abstracts the essential mathematical properties of excitation and propagation from the electrochemical details of sodium and potassium ion flow. As such, it remains a realistic model of neural dynamics while being more tractable in relation to analysis and visualisation than the higher dimensional HH model (with which it is upwardly compatible). The equations used are derived from those describing a van der Pol non-linear relaxation oscillator, hence it is sometimes also referred to as the Bonhoeffer–van der Pol model.

Neural circuits involving coupled FHNs have particularly rich oscillatory dynamics which can become chaotic and multistable (Asai, Nomura, & Sato, 2000; Yanagita, Ichinomiya, & Oyama, 2005). Hence, because of their relative tractability, they have been used in simulation studies aimed at better understanding the functional role of chaotic dynamics in the nervous system. A particular form of coupled FHN neuron circuit, introduced by Asai, Nomura, Sato, et al. (2003), has proven very useful as a model of central pattern generator (CPG) units in the nervous system, used in motor behaviours. For instance, such circuits have been used to model human interlimb coordination, successfully reproducing clinical data from studies of patients with Parkinsons disease, including normal and disordered movements (Asai, Nomura, Abe, et al., 2003; Asai, Nomura, Sato, et al., 2003). They have also been used to model the development and learning of limb coordination (Kuniyoshi & Sangawa, 2006; Kuniyoshi et al., 2007), including with an approach which exploits controllable chaotic dynamics to learn stable and efficient gaits for walking and swimming (Shim & Husbands, 2012, 2015), which can also be applied in robotics.

Asai et al. (2000) and Asai, Nomura, Sato, et al. (2003) provided very useful, detailed bifurcation analyses of these coupled FHN motor circuits which showed how the chaoticity of the system could vary under the influence of control parameters. Other bifurcation analyses of related, but more simply coupled, versions of the circuits followed, highlighting different aspects of the dynamics (Ciszak, Euzzor, Arecchi, & Meucci, 2013; Hoff, dos Santos, Mancheina, & Albuquerque, 2014) or focusing on more abstract, less biologically motivated analysis (Yanagita et al., 2005). In this article, we aim to extent Asai, Nomura, Sato, et al.'s (2003) original work on the more complex, strongly biologically motivated, form of the FHN coupled CPG circuits. Unlike the other models mentioned above, this includes variables representing tonic descending command signals and a coupling to the refractory variables

(from x to y in the equations in the next section). While the original, partly qualitative, analysis was highly informative, until now a more detailed, quantitative dynamical analysis of this important system, particularly with regard to characterising the attractor types and mapping regions of chaotic dynamics, has not been available. In this short article, we fill that gap by conducting an elaborate search of possible attractors as well as calculating dynamical quantities, such as the largest Lyapunov exponents (LLEs), at a fine resolution over the most important areas of parameter space, to build a more detailed picture of the dynamical regimes of the system.

Identifying chaos in a given dynamical system is important both for accurately modelling and analysing the system. The LLE is one of the few mathematical measures of a system's chaoticity and is used in this work, together with Lyapunov spectra, to properly characterise the possible behaviours of the coupled FHN system. Different systems all of which exhibit seemingly irregular behaviours cannot be automatically grouped together as chaotic, since they might be either multiperiodic or quasiperiodic, or even show long transient behaviours (which appear chaotic) before settling into a stationary state such as a fixed point or limit cycle. Thus, a mathematical rigorous analysis, done here for the first time, is one significant contribution beyond the previous work because it allows an accurate characterisation of behaviour of the FHN system.

The greater understanding thus provided is intended to help future studies on the roles of chaotic dynamics in biological motor control, and in the application of such circuits in robotics; particularly by giving a deeper insight into how input signals and control parameters shape the system's dynamics.

2. The Model

We consider two identical Fitzhugh–Nagumo neuron (FHN) equations bidirectionally coupled by output-to-all connections (Asai et al., 2000). Asai's model of two coupled FHNs can be described by the output variable x and the recovery variable y as follows

$$\dot{x}_1 = c\left(x_1 - \frac{x_1^3}{3} - y_1 + z_1\right) + \delta(x_2 - x_1) \qquad (1)$$

$$\dot{y}_1 = \frac{1}{c}(x_1 - by_1 + a) + \varepsilon x_2 \qquad (2)$$

$$\dot{x}_2 = c\left(x_2 - \frac{x_2^3}{3} - y_2 + z_2\right) + \delta(x_1 - x_2) \qquad (3)$$

$$\dot{y}_2 = \frac{1}{c}(x_2 - by_2 + a) + \varepsilon x_1 \qquad (4)$$

where the equation constants are $a = 0.7$, $b = 0.675$ and $c = 1.75$, which are set such that the neurons

exhibit biologically plausible dynamics (empirically determined through sweeps of parameter space by the current and other authors (Asai, Nomura, Sato, et al., 2003; Shim & Husbands, 2012)). The system employing these values has already successfully reproduced human interlimb coordination both in normal and pathological states (Asai, Nomura, Sato, et al., 2003) and successfully transferred to modelling the development of limb coordination (Kuniyoshi et al., 2007) and to the development of adaptive, chaos-driven neural mechanisms used in locomotion learning (Shim & Husbands, 2012, 2015). The coupling strengths are set to $\delta = 0.013$ and $\varepsilon = 0.022$ after similar empirical explorations. These were found to be the best values of the constants, although broadly similar behaviour can be exhibited with values close to these. z_1 and z_2 represent tonic descending command signals from pathways entering the neural motor centres, and they should be considered as the bifurcation parameters of the system. It had been shown that the model exhibits a wide range of dynamics from different phase locked and quasiperiodic oscillations to chaotic orbits as the combination of the two control parameters changes (Asai, Nomura, Abe, et al., 2003; Asai, Nomura, Sato, et al., 2003). In particular, the dynamics of the coupled systems is mainly influenced by the degree of asymmetry between the two neurons which is instantiated by the difference between z_1 and z_2. The presence of both the tonic descending commands and the variable half-centre asymmetry they can influence are the key elements for assessing the biological implication of the model, as they mimic hierarchical and coherent control structures of the nervous system. This is in contrast to the other simpler models mentioned above, which do not include descending signals and tend to focus only on extreme cases of coupling: unidirectional and perfectly symmetrical bidirectional (Hoff et al., 2014).

The coupled FHN model described by the equations above can either be used to model at the level of single neurons, or, as in (Asai, Nomura, Sato, et al., 2003), at the level of neural populations. As a single spiking neuron model, the variables x and y represent the membrane potential and refractoriness of a cell. When used at the population level, x and y can be regarded as the activities of excitatory and inhibitory cell populations, respectively. In this case, the coupling between x variables can be interpreted as a two-way connection between the two excitatory populations, and x-to-y couplings as the excitatory connections from an excitatory population to an inhibitory population. In either case, the system can be considered as a realisation of the half-centre model with reciprocal inhibition (Brown, 1914), which is still widely accepted as the underlying mechanism of many biological CPGs.

We extend Asai, Nomura, Abe, et al. (2003; Asai et al., 2000) original analyses by investigating two aspects of particular interest. The first analysis is intended to produce a detailed map of chaotic regions on the parameter space. Asai, Nomura, Sato, et al. (2003) explored the dynamics of the model, as applied to describing human interlimb coordination, by varying the two bifurcation parameters and categorised the dynamics into different groups using a hierarchical clustering method which measured multiple features of oscillatory patterns such as the variance of amplitude modulation and the mean relative phase. From these measures, they classified the oscillatory patterns into different categories based on the distinct interlimb coordinations obtained from clinical data. Among these categories, they roughly indicated the region of chaotic dynamics of the model on a $z - dz$ parameter space where $z_1 = z$ and $z_2 = z + dz$. However, this region was determined based on a partly qualitative waveform clustering method, mainly by identifying the irregular transition of relative phase, rather than measuring LLEs which are widely accepted as an indicator of chaos. Thus, in this article, we investigate these dynamics in more detail, to give a more precise, quantitative characterisation, by measuring LLEs over various regions of the $z - dz$ space, including those which were classified as the most chaotic in the previous rough characterisation.

The second analysis investigates a particularly interesting narrow range of z in the tonic symmetry case ($z_1 = z_2$), which is the early parameter region near the Hopf bifurcation of FHNs. In contrast to the region where the value of z is far from the Hopf bifurcation point, the early region exhibits more complex bifurcation phenomena including symmetry breaking, Hopf branches, double cycles, and period doubling routes to chaos despite the symmetry of the coupled system (Asai et al., 2000). While the previous work pointed out a few representative attractors (in-phase, anti-phase and out-of-phase) in this range by providing a bifurcation diagram on a Poincaré section, we have discovered that there are various kinds of distinct oscillatory solutions *coexisting* with each other (e.g. periodic solutions of different periods, 2-torus and multiple chaotic solutions) over a wide range of z within this region. Specifically, we focus on the parameter range $z_s < z < z_a$, where z_s is the point where the stable and unstable oscillatory solutions begin to appear and bifurcate (due to the subcritical Hopf bifurcation) and z_a is the point such that for $z > z_a$, the system only exhibits one or both of the typical solutions of the general two identical coupled oscillators, that is, anti-phase and in-phase oscillations.

3. Results

3.1. LLE map of the chaotic region

A map of the LLEs of the coupled FHNs on the selected parameter region is shown in Figure 1. The LLEs were calculated using a numerical method by
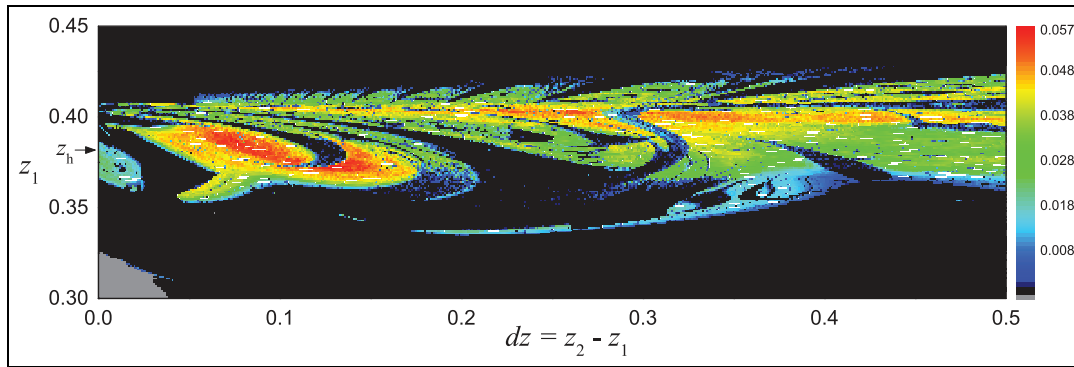
Figure 1. LLE map on $dz - z_1$ parameter space. The parameter area includes and extends the previously suggested region of possible chaotic solutions (the diagonal region (c) of Figure 6 in Asai, Nomura, Abe, et al. (2003)). The calculation was performed over the area with an interval of 0.001 for both axes. Due to the finite duration of the calculation, only values larger than $\lambda_1 > 5 \times 10^{-4}$ were plotted as positive LLEs. The arrow indicates the Hopf bifurcation point $z_h \approx 0.3824$ of a single uncoupled FHN. Non-oscillatory steady states are shown in grey at the lower left corner.

Wolf, Swift, Swinney, and Vastano (1985) over the belt-shaped area covering the possible chaotic region identified in the previous study (region (c) in Figure 6 of Asai, Nomura, Abe, et al., 2003). Note that the region analysed for chaos is significantly expanded from the previous one by increasing the range of dz up to 0.5 ($dz < 0.3$ in the previous work). For compact visualisation of this diagonal region of interest, it is plotted using z_1 versus positive values of dz, where $dz = z_2 - z_1$ and z_1 is the smaller of the two z values.

The model equations were numerically updated using Runge–Kutta fourth-order integration with a time-step of 0.001 s for 2×10^7 iterations, which is considered long enough to ensure the precision of the final LLEs up to a few floating point digits, while the satisfactory convergence of LLEs was normally observed before 5×10^6 iterations. The calculation of the trajectory separation and renormalisation (back to the initial distance of 1×10^{-7}) was done at every time-step.

The precise map clearly shows that the sub-regions with positive LLEs (indicating chaos) all lie within the hypothesised area, thus supporting and reinforcing the previous work on identifying the chaotic region. Observing the horizontally stretched braid of the chaotic area indicates that the chaotic dynamics mainly take place around $z_1 = z_h \approx 0.3812$ (i.e. the Hopf bifurcation point of a single FHN) over the whole range of dz, which means that the smaller of FHN's two control parameters (z_1) stays near its critical state (z_h), which is analogous to chaos at the border of criticality (Medvedev & Yoo, 2008).

As shown in the previous study (Asai, Nomura, Abe, et al., 2003), the difference in the oscillation amplitudes of the two neurons in a coupled circuit represents the asymmetry of the solutions and is crucial for the non-periodic patterns. In chaotic solutions, the amplitudes of the two FHNs in both the tonic symmetric and asymmetric cases show similar patterns: the variance of

the amplitude of the FHN with smaller z is much larger than the FHN with bigger z, while its maximum amplitude is smaller. From this observation, one possible intuition about the mechanism of chaos can be drawn – at least in the case of tonic asymmetry – by looking at each oscillator separately. The limit cycle of a single uncoupled FHN with smaller z near a Hopf bifurcation point is smaller and more vulnerable to external perturbation (for instance, if the orbit is perturbed by an impulse in a radial direction, then it takes longer to return to the original limit cycle). If it is coupled reciprocally with a second oscillator which has larger z (thus having a bigger and more stable limit cycle), then the smaller limit cycle of the first oscillator distorts more easily, whereas the larger limit cycle remains almost intact with little variance; this becomes a major source of complexity for chaotic solutions.

3.2. Multistable solutions in the symmetric case near Hopf bifurcations

Next let us illustrate the detailed ecology of multiple attractors in the system with tonic symmetry ($dz = 0$, $z_1 = z_2 = z$), which emerge in the narrow range of z near Hopf branches. First, we performed an elaborate manual search for all the coexisting stable attractors in the parameter range of interest by running the simulation at each z several times with different initial conditions. Then, we categorised the attractors thus discovered by referring to the bifurcation diagrams in the previous work (Asai et al., 2000; Asai, Nomura, Sato, et al., 2003). The parameter range of interest is $z_s \leqslant z \leqslant z_a$, where $z_s = 0.3262$ is the point near the first Hopf branch at which stable in-phase oscillations begin to appear from a non-oscillatory state, and $z > z_a = 0.4075$ is the region where all the interesting attractors disappear and only anti-phase oscillations remain stable, along with an unstable in-phase solution, until it is accompanied by a stable in-phase
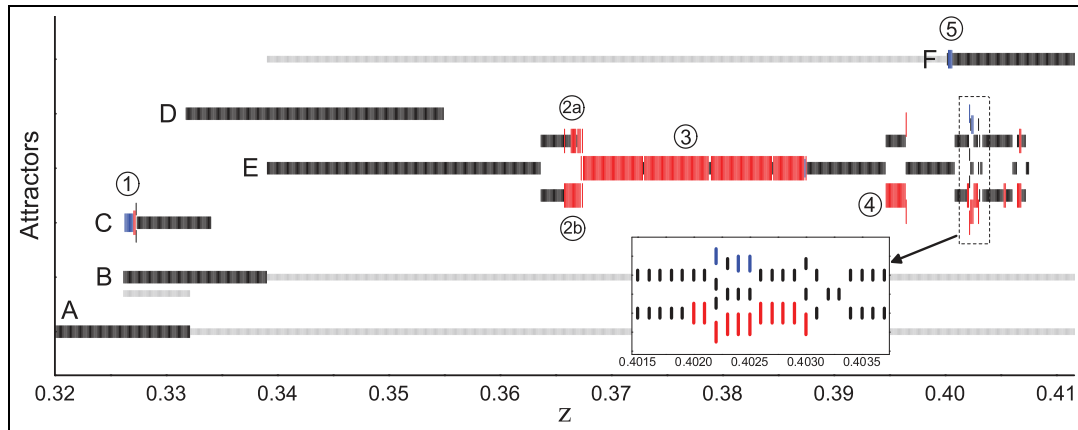
Figure 2. Inhabitancy diagram of different attractor groups versus the control parameter $z_1 = z_2 = z$. At each value of z, the coexistence of attractors was plotted using vertical bars with different colours and sizes according to the signs of their Lyapunov spectra; (black) n-period oscillation $\{0,-,-,-\}$, (blue) 2-torus $\{0,0,-,-\}$ and (red) chaos $\{+,0,-,-\}$. Inset shows a magnification of the region surrounded by the dashed box. See Table 1 for the details of different n-periodic solutions.

solution again. Since the analytically solved Hopf bifurcation point of a single uncoupled FHN is $z_h \approx 0.3812441$, it can be seen that most of the interesting bifurcation dynamics in this range results from the interaction of two half-centres. The control parameters were scanned with an interval of 0.0001, such that a total of 814 parameters values were investigated. Also, all the stable attractors which exhibited complex non-periodic orbits were examined using their Lyapunov spectrum in order to identify their quasiperiodic/chaotic properties.

Figure 2 shows all the stable attractors manually found within the prescribed parameter range, together with illustrations of a few unstable solutions (shown as thin grey lines) which were incorporated from the analysis in the previous studies (Asai et al., 2000; Asai, Nomura, Sato, et al., 2003). The attractor solutions were categorised into six groups (A–F) according to their representative trajectories in state space. Due to the left–right symmetry of two half-centres, any solution having different amplitudes between two FHNs caused by symmetry-breaking bifurcation has another coexisting mirrored solution. The two are interchangeable by flipping either the initial conditions or the indices of two FHNs. Thus, we considered only one of the mirrored twins as an individual solution for categorisation. These groups are D and E, whereas A, B, C, and F are the inherently symmetric solutions.

There is no oscillatory solution where $z<z_s = 0.3262$, only stable equilibrium (fixed points) exists (group A in Figure 2). As the control parameter increases beyond z_s, stable and unstable in-phase solutions emerge simultaneously by double-cycle bifurcation and they coexist with stable equilibriums (group B) until the unstable in-phase solutions coalesce into unstabilised equilibrium which correspond to subcritical Hopf bifurcation in a two-dimensional subspace of the system (Asai, Nomura, Sato, et al., 2003). In addition, another new stable solution, which was not shown in the previous

studies, emerges immediately after this double cycle bifurcation; this is the family of 2-period near-in-phase oscillations whose trajectory on (x_1, x_2) space is butterfly shaped (group C). Beyond the in-phase Hopf branching, a slightly out-of-phase solution occurs (group D) having highly asymmetric amplitudes between two FHNs, which is similar to one of the solutions shown in previous work on the tonic asymmetric case ((a4) and (a5) in Figure 2 of Asai, Nomura, Abe, et al. (2003)), but in this case, the smaller limit cycle has a two-period orbit. The stable in-phase solution changes its stability at $z = 0.3391$, giving birth to a family of major out-of-phase solutions (group E) which has a rich repertoire of dynamics over a wide range of parameters, including the period doubling route to chaos as well as the coexistence of multiple variations of similar solutions (e.g. at $z = 0.4022$) even with different quantitative measures (i.e. chaoticity). Finally, the anti-phase solution (group F), born at the second Hopf branch, becomes stable at $z = 0.4002$ and persists (as the sole solution) far beyond z_a.

Figures 3 to 8 show a deeper investigation of a few selected parameter ranges using Lyapunov spectra and attractor trajectories, which looks into sub-regions 1–5 in Figure 2 to identify quasiperiodic or chaotic solutions (shown as blue and red bars). These regions were chosen for further analysis because their dynamics are particularly rich and complex. The Lyapunov spectrum was calculated by the discrete QR-based method (Dieci, Russell, & Van Vleck, 1997) for 5×10^7 iterations where the decomposition of the updated variational matrix by the Gram–Schmidt procedure was performed at every integration step. Other simulation parameters were the same as in the previous LLE calculation.

Sub-regions 1 and 5 in groups C and F show initially complex orbits (multiperiodic, quasiperiodic and even chaotic) right after the birth of each group. The trajectories swirl around an unstable periodic solution
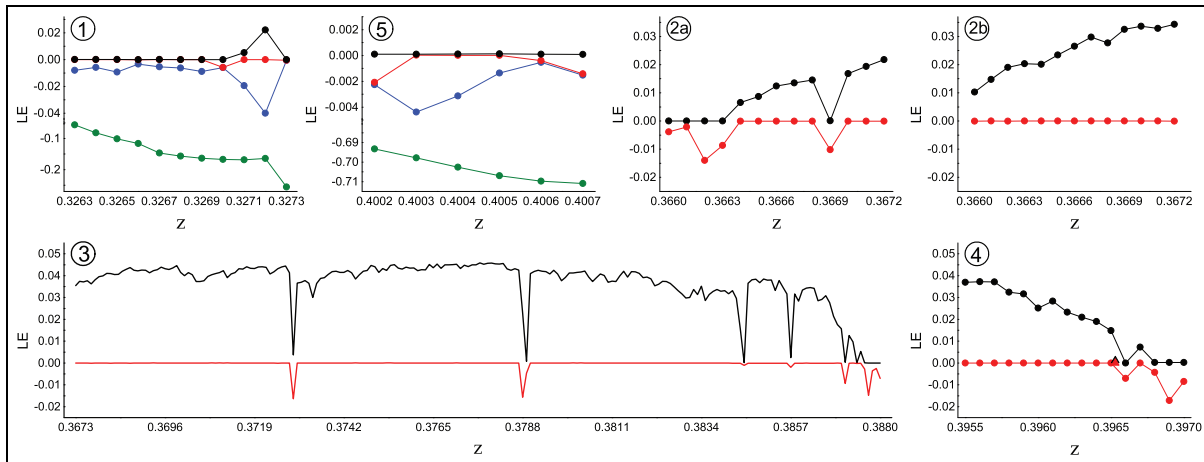
Figure 3. Lyapunov exponents of the specified regions in Figure 2. The four LEs ($\lambda_1 > \lambda_2 > \lambda_3 > \lambda_4$) are coloured as black, red, blue and green, respectively.
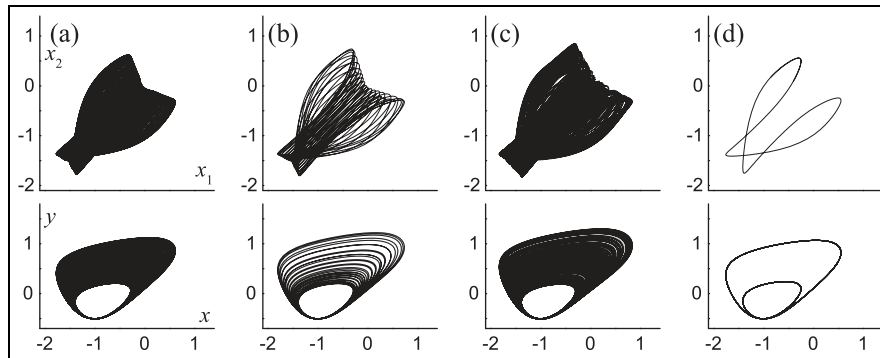

Figure 4. Examples of trajectories in group C. The pair of plots for each column shows the orbits on (x_1, x_2) and (x, y) planes (black: (x_1, y_1), grey: (x_2, y_2)) for the corresponding solution: (a) 2-torus at $z = 0.3267$, (b) 34-period at $z = 0.3270$, (c) chaos at $z = 0.3272$ and (d) 2-period at $z = 0.3274$, which is the representative trajectory of group C.

('skeleton'), which is later stabilised to a representative solution of the corresponding group as z increases. Both the first and second Lyapunov exponents (LEs) of quasiperiodic oscillations are virtually zero (Figure 3(1) and (5)), and their Poincaré maps (Figure 8(a) and (c)) form one-dimensional closed trajectories in three-dimensional space, which indicates that they are 2-torus. While the early quasiperiodic solutions of the anti-phase family (group F) seem to follow a typical torus bifurcation process, some of the early dynamics of group C (2-period butterfly) exhibit chaos (positive λ_1 and a cracked Poincaré map in Figure 8(b)).

In the parameter space under investigation, the solution group E can be seen as the major solution group caused by symmetry-breaking bifurcation. They are a family of out-of-phase solutions who tend towards more complex dynamics. A variety of out-of-phase solutions with different periodicities coexist and coalesce by branching into sub-groups (e.g. (2a) and (2b) in Figure 2), which go through their own period doubling

cascades creating different chaotic solutions that preserve their trajectory characteristics to some degree. A few parameter points near the last period of the group (inset in Figure 2) show a particularly rich coexistence of various solutions. For example, the system with $z = 0.4022$ exhibits the coexistence of four distinct out-of-phase patterns with different periodicities; a total of five stable attractors (four from group E and one from group F) coexist at this parameter value (Table 1).

4. Discussion

We presented a rigorous analysis of the dynamical behaviours of a system of two coupled FHNs with descending command signals, focusing on regions with rich dynamics of potential use in the generation of motor behaviours. Expanding on the prior work of (Asai, Nomura, Abe, et al., 2003; Asai, Nomura, Sato, et al., 2003), we developed a more detailed and more quantitative analysis. In so doing, we identified a
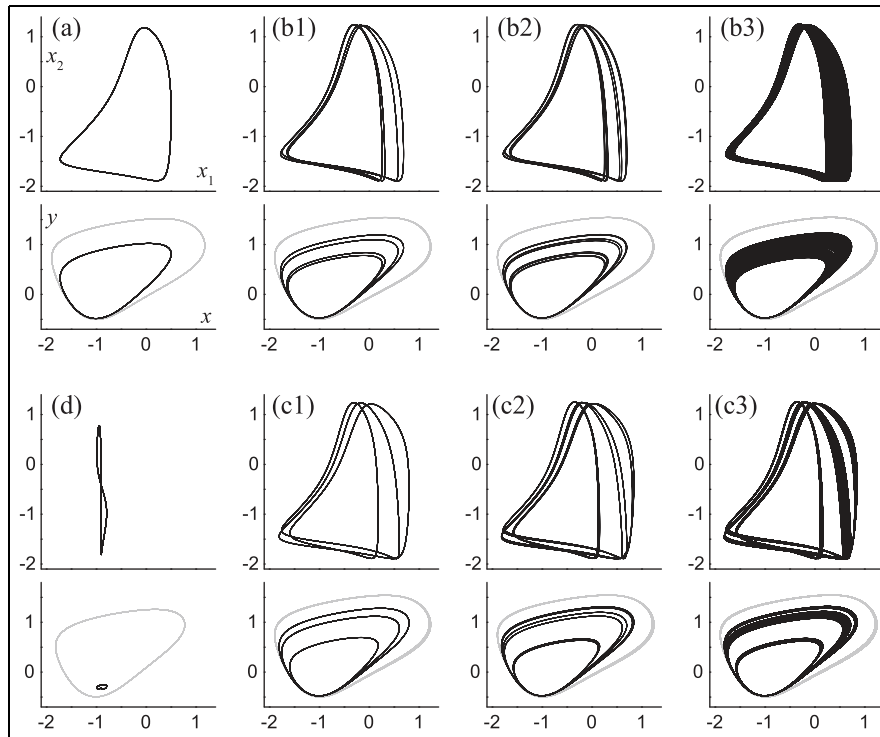
Figure 5. Examples of trajectories in group E (out-of-phase solution family). An example of group D (highly asymmetric amplitudes) is shown together at the lower left corner for convenience. (a) 1-period at $z = 0.3550$. (b1–b3) An example of the period doubling route to chaos of the first solution branch in Figure 2-(2a); 4-period at $z = 0.3252$, 8-period at $z = 0.3256$ and chaos at $z = 0.3266$. (c1–c3) Period doubling cascade of the second branch (2b); 3-period at $z = 0.3238$, 6-period at $z = 0.3260$ and chaos at $z = 0.3266$. Note that the two different chaotic solutions (b3 and c3) bifurcated from each branch coexist at $z = 0.3266$.
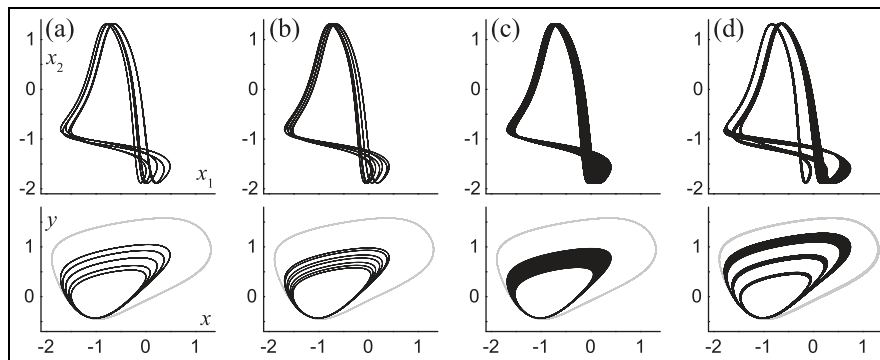

Figure 6. Four different solutions coexisting at $z = 0.4022$. (a) 5-period, (b) 7-period, (c) 2-torus and (d) Chaos.

narrow region of parameter space of particular interest, replete with chaotic and multistable dynamics.

But outside of this tight region, there were only two, unremarkable and uninteresting, solutions: in-phase and anti-phase oscillations. The region of special interest, the only one showing complex coexisting solutions, lies at the border of criticality, very close to the Hopf bifurcation point of a single FHN ($z_h \approx 0.3824$). In biological terms, in this state, an individual FHN is at the border of two important types of oscillatory (CPG) behaviour: half-centre (requiring a reciprocally linked

partner FHN) and pacemaker (having intrinsic oscillatory dynamics of its own). Dynamics poised on this border can be exploited in a powerful way in the development, learning and generation of motor behaviours (Kuniyoshi et al., 2007; Shim & Husbands, 2015), and the analysis in this article will help to refine such research. For instance, it was demonstrated that chaotic dynamics emerging spontaneously from interactions between neural circuitry, bodies and environments can be used to power a kind of search process (chaotic search) enabling an embodied system to explore its
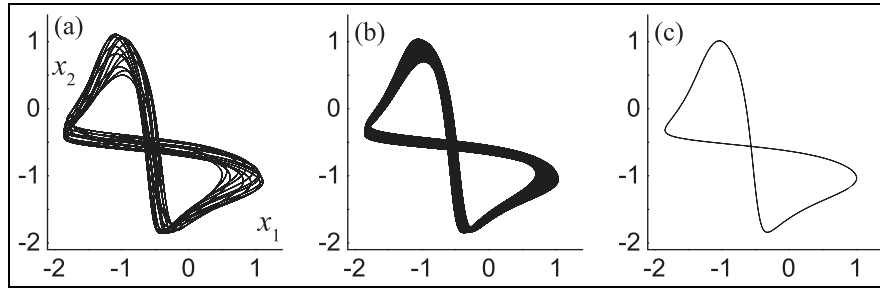
Figure 7. Examples of trajectories in group F (anti-phase solutions): (a) 13-period at $z = 0.4002$, (b) 2-torus at $z = 0.4004$ and (c) 1-period representative solution at $z = 0.4067$.
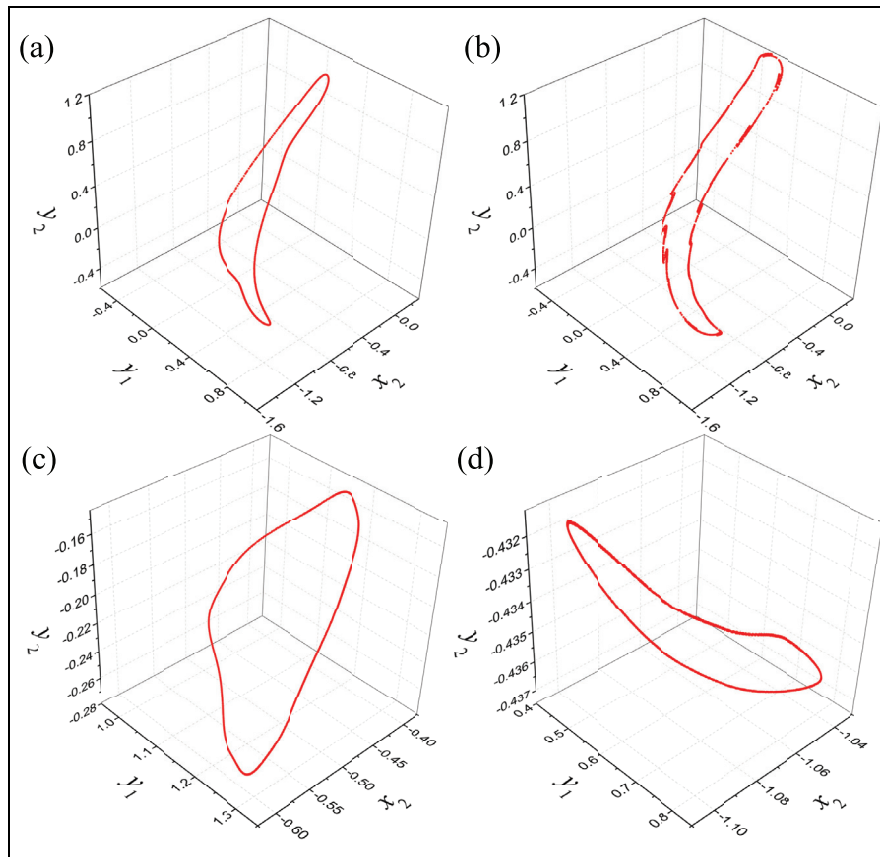

Figure 8. Example of the Poincaré maps for torus and chaotic solutions. The points of the maps were plotted on (y_1, x_2, y_2) space whenever x_1 crosses the hypersurface $x_1 = -1$ in the positive direction: (a) 2-torus in group C at $z = 0.3267$, (b) chaos in group C at $z = 0.3271$, (c) 2-torus in group F at $z = 0.4003$ and (d) 2-torus in group E at $z = 0.4022$ (i.e. one of the four coexisting solutions).

own possible motor behaviours (Kuniyoshi & Suzuki, 2004). This idea has been advanced by showing how to harness chaos in a general goal-directed way such that desired adaptive sensorimotor behaviours can be explored, captured and learned (Shim & Husbands, 2012, 2015). Key to this adaptive method is the control of chaos in coupled FHN neurons through changes to the z parameter by actively linking it to a performance measure which feeds back into the system. Chaos is increased, stimulating more exploration, when the performance level is low and is reduced as performance increases, turning off as the system stabilises on a high performing attractor. The detailed analysis of the coupled FHN dynamics presented here allows us to see in greater detail than previously how changes in z shape the dynamics and which regions of parameter space have the richest dynamics, most amenable to chaotic search. By biasing the system towards such regions the adaptive mechanisms can be made more efficient. Although the dynamics of these systems were referred

Table 1. All existing stable attractors and their periodicities for values of *z*, organised in terms of the groups A–F. The numbers *n* in the columns represent stable *n*-period oscillations (zero indicates a stable equilibrium), and the letters indicate (T): 2-torus and (C): chaotic. Each column represents the corresponding attractor group as shown in Figure 2, where the coexistence of different solutions within the same group is shown as multiple entries separated by commas. The period of the solution marked with an asterisk (*) was counted up to 120 due to the precision limit.

z	A	B	C	D	E	F
≤0.3261	0					
0.3262	0	1				
0.3263–0.3269	0	1	T			
0.3270	0	1	34			
0.3271	0	1	C			
0.3272	0	1	C			
0.3273	0	1	2,8			
0.3274–0.3317	0	1	2			
0.3318–0.3321	0	1	2	1		
0.3322–0.3340		1	2	1		
0.3341–0.3390		1		1		
0.3391–0.3549				1	1	
0.3550–0.3583					1	
0.3584–0.3636					2	
0.3637–0.3639					2,3	
0.3640–0.3652					4,3	
0.3653					4,6	
0.3654–0.3656					8,6	
0.3657					16,6	
0.3658					C,6	
0.3659					20,6	
0.3660					C,6	
0.3661–0.3662					C,12	
0.3663					C,16	
0.3664–0.3668					C,C	
0.3669					C,9	
0.3670–0.3672					C,C	
0.3673					C	
0.3674					C,7	
0.3675–0.3728					C	
0.3729					9	
0.3730–0.3787					C	
0.3788					8	
0.3789					32	
0.3790–0.3844					C	
0.3845					8	
0.3846–0.3856					C	
0.3857					48	
0.3858–0.3870					C	
0.3871					15	
0.3872–0.3873					C	
0.3874					48	
0.3875					C	
0.3876					24	
0.3877–0.3878					12	
0.3879–0.3892					6	
0.3893–0.3946					3	
0.3947–0.3953					3,C	
0.3954–0.3964					C	
0.3965					C,C,5	
0.3966					12	
0.3967					C	
0.3968					16	
0.3969–0.3970					8	
0.3971–0.3983					4	
0.3984–0.4001					2	
0.4002					2	13
0.4003–0.4006					2	T

(continued)

Table1. Continued

z	A	B	C	D	E	F
0.4007–0.4008					2	I
0.4009–0.4014					2,3	I
0.4015–0.4018					2,6	I
0.4019					2,12	I
0.4020					11,C	I
0.4021					9,C	I
0.4022					5,7,C,T	I
0.4023					5,7,C	I
0.4024–0.4025					5,C,T	I
0.4026–0.4029					5,C	I
0.4030					24,16,C	I
0.4031					12,16	I
0.4032–0.4033					12	I
0.4034–0.4042					6,4	I
0.4043–0.4052					3,4	I
0.4053–0.4054					3,C	I
0.4055–0.4057					3,14	I
0.4058–0.4059					3,7	I
0.4060					>120*,7	I
0.4061–0.4062					7	I
0.4063					13	I
0.4064					6	I
0.4065					4,C	I
0.4066					22,C	I
0.4067–0.4068					C,C	I
0.4069					8,10	I
0.4070					4,5	I
0.4071–0.4072					4,10	I
0.4073–0.4075					4	I
0.4076⩽						I

to as chaotic in previous publications (because bifurcation analysis strongly pointed in that direction), now with the more rigorous analysis provided by this article, we can safely say they truly are chaotic.

The detailed LLE map of the chaotic region of the coupled FHN system, and the Lyapunov spectra for more detailed investigation of some parameter ranges, were calculated using well-accepted numerical methods (Dieci et al., 1997; Wolf et al., 1985) using a fine integration time-step and a large number of iteration to ensure convergence of all calculations. Numerical methods were used since for this highly non-linear system, the relevant equations are not analytically tractable. Although there can always be slight doubts about numerical calculations, the methods used here are uncontroversial and produced highly stable results. If (as is widely done) we define a system as chaotic (in a subset S of state space), if it shows (1) sensitive dependence on initial conditions and (2) S is bounded so as to exclude the trivial case of an unstable linear system whose trajectories diverge exponentially for all times, then the system described in this article exhibits chaos. Condition (1) is satisfied if the properly calculated LLE is positive, which is the case for the system in the regions depicted in Figure 1, and condition (2) is clearly

satisfied in this case, so we are justified in referring to the neural dynamics as chaotic. However, ultimately the systems of most interest for understanding adaptive behaviour are embodied. Here, the overall dynamics involve multiple brain–body–environment interactions and the analysis of such dynamics is significantly harder. A study of the overall dynamics of a fully embodied system with a coupled FHN–based nervous system (such as in Shim & Husbands, 2015) will be the subject of a future paper; preliminary results suggest we can refer to the whole system as chaotic.

Although the elaborate categorisation of different stable solutions in the tonic symmetry case were presented by looking into a narrow parameter region in detail, they were manually found by observing the evolution of trajectories starting from various random initial conditions up to a few 100 points. This method inevitably introduces an element of coarseness into the exploration of possible basins of attraction in a four-dimensional space. One future direction would be to employ a clustering analysis similar to Asai, Nomura, Abe, et al. (2003), but specialised for detecting more detailed oscillatory patterns including the number of oscillation periods, *n*-torus and chaotic attractors, incorporated by Lyapunov analysis. For example, it is difficult to distinguish between the

2-torus and chaotic attractors in group C or the different chaotic orbits (and torus) in group E because of their similarities in the evolution of relative phases and the amplitude variances.

By presenting a more detailed picture of the coupled FHN system's dynamics, particularly in the region of high complexity, our intention is to aid future studies on the roles of chaotic dynamics in biological motor control, and in the application of such mechanisms in robotics, by providing the most promising parameter ranges to pursue.

The intrinsic stability and dynamical structure of non-chaotic and chaotic systems are different even if their orbits seem similarly irregular, which may well lead to different behaviours when such systems are used for robot control under the influence of external forces/control signals and/or noise. Hence, when applying these ideas in biorobotics, it is important to have a rigorous understanding of the dynamics as provided by this article.

Declaration of Conflicting Interests

Funding

References

Aihara, K., & Matsumoto, G. (1982). Temporally coherent organization and instabilities in squid giant axons. *Journal of Theoretical Biology*, *95*, 697–720.

Asai, Y., Nomura, T., Abe, K., & Sato, S. (2003). Classification of dynamics of a model of motor coordination and comparison with Parkinson's disease data. *Biosystems*, *71*, 11–21.

Asai, Y., Nomura, T., & Sato, S. (2000). Emergence of oscillations in a model of weakly coupled two Bonhoeffer-van der Pol equations. *Biosystems*, *58*, 239–247.

Asai, Y., Nomura, T., Sato, S., Tamaki, A., Matsuo, Y., Mizukura, I., & Abe, K. (2003) A coupled oscillator model of disordered interlimb coordination in patients with Parkinson's disease. *Biological Cybernetics*, *88*, 152–162.

Brown, T. G. (1914). On the nature of the fundamental activity of the nervous centres; together with an analysis of the conditioning of rhythmic activity in progression, and a theory of the evolution of function in the nervous system. *Journal of Physiology*, *48*, 18–46.

Ciszak, M., Euzzor, S., Arecchi, F. T., & Meucci, R. (2013). Experimental study of firing death in a network of chaotic Fitzhugh-Nagumo neurons. *Physical Review E*, *87*, 022919.

Dieci, L., Russell, R., & Van Vleck, E. (1997). On the computation of Lyapunov exponents for continuous dynamical systems. *SIAM Journal on Numerical Analysis*, *34*, 402–423.

Fitzhugh, R. (1961). Impulses and physiological states in theoretical models of nerve membrane. *Biophysical Journal*, *1*, 445–466.

Freeman, W. J., & Viana Di Prisco, G. (1986). EEG spatial pattern differences with discriminated odors manifest chaotic and limit cycle attractors in olfactory bulb of rabbits. In G. Palm and A. Aertsen (Eds.), *Brain theory* (pp. 97–119). London, England: Springer-Verlag.

Guevara, M. R., Glass, L., Mackey, M. C., & Shrier, A. (1983). Chaos in neurobiology. *IEEE Transactions on Systems, Man, and Cybernetics*, *13*, 790–798.

Hodgkin, A., & Huxley, A. (1952). A quantitative description of membrane current and its application to conduction and excitation in nerve. *Journal of Physiology*, *117*, 500–544.

Hoerzer, G. M., Legenstein, R., & Maass, W. (2014). Emergence of complex computational structures from chaotic neural networks through reward-modulated Hebbian learning. *Cerebral Cortex*, *24*, 677–690.

Hoff, A., dos Santos, J. V., Mancheina, C., & Albuquerque, H. A. (2014). Numerical bifurcation analysis of two coupled Fitzhugh-Nagumo oscillators. *European Physical Journal B*, *87*, 151.

Korn, H., & Faure, P. (2003). Is there chaos in the brain? II. Experimental evidence and related models. *Comptes Rendus Biologies*, *326*, 787–840.

Kuniyoshi, Y., & Sangawa, S. (2006). Early motor development from partially ordered neural-body dynamics: Experiments with a cortico-spinal-musculo-skeletal model. *Biological Cybernetics*, *95*, 589–605.

Kuniyoshi, Y., & Suzuki, S. (2004). *Dynamic emergence and adaptation of behavior through embodiment as coupled chaotic field*. Paper presented at Proceedings of IEEE International Conference on Intelligent Robots and Systems Sendai, Japan. 28 September - 2 October 2004 (pp. 2042–2049). New York, NY: IEEE.

Kuniyoshi, Y., Yorozu, Y., Suzuki, S., Sangawa, S., Ohmura, Y., Terada, K., & Nagakubo, A. (2007). Emergence and development of embodied cognition: A constructivist approach using robots. *Progress in Brain Research*, *164*, 425–445.

Medvedev, G. S., & Yoo, Y. (2008). Chaos at the border of criticality. *Chaos*, *18*, 033105.

Nagumo, J., Arimoto, S., & Yoshizawa, S. (1962). An active pulse transmission line simulating nerve axon. *Proceedings of the IRE*, *50*, 2061–2071.

Ohgi, S., Morita, S., Loo, K., & Mizuike, C. (2008). Time series analysis of spontaneous upper-extremity movements of premature infants with brain injuries. *Physical Therapy*, *88*, 1022–1033.

Rapp, P., Zimmerman, I., Albano, A., Deguzman, G., & Greenbaun, N. (1985). Dynamics of spontaneous neural activity in the simian motor cortex: The dimension of chaotic neurons. *Physics Letters A*, *110*, 335–338.

Shim, Y., & Husbands, P. (2012). Chaotic exploration and learning of locomotion behaviours. *Neural Computation*, *24*, 2185–2222.

Shim, Y., & Husbands, P. (2015). Incremental embodied chaotic exploration of self-organized motor behaviors with proprioceptor adaptation. *Frontiers in Robotics and AI*, *2*, 7.

Skarda, C., & Freeman, W. (1987). How brains make chaos in order to make sense of the world. *Behavioral and Brain Sciences*, *10*, 161–195.

Sussillo, D., & Abbott, L. F. (2009). Generating coherent patterns of activity from chaotic neural networks. *Neuron*, *63*, 544–557.

Terman, D., & Rubin, J. (2007). Neuronal dynamics and the basal ganglia. *SIAM News*, *40*. Retrieved from https://archive.siam.org/news/news.php?id = 1092

Wolf, A., Swift, J. B., Swinney, H. L., & Vastano, J. A. (1985). Determining Lyapunov exponents from a time series. *Physica D: Nonlinear Phenomena*, *16*, 285–317.

Wright, J., & Liley, D. (1996). Dynamics of the brain at global and microscopic scales: Neural networks and the EEG. *Behavioral and Brain Sciences*, *19*, 285–320.

Yanagita, T., Ichinomiya, T., & Oyama, Y. (2005). Pair of excitable Fitzhugh-Nagumo elements: Synchronization, multistability, and chaos. *Physical Review E*, *72*, 056218.

About the Authors

Yoonsik Shim obtained a Doctral Degree in Informatics from University of Sussex. He is a member of the CCNR. His research interests are focused on bio-inspired adaptive robotics, computational neuroscience, chaotic neurodynamics, self-organisation, and evolutionary robotics.

Phil Husbands is a research professor of Artificial Intelligence and co-founder of the CCNR, University of Sussex. His research interests include biologically inspired adaptive robotics, evolutionary systems, computational neuroscience, history and philosophy of AI and cybernetics, machine learning and creative systems.